European Journal of Mechanics B/Fluids 28 (2009) 670–676

Contents lists available at ScienceDirect

European Journal of Mechanics B/Fluids

journal homepage: www.elsevier.com/locate/ejmflu

Capillary cavity flow past a circular cylinder

Bum-Sang Yoon, Yuriy A. Semenov*

School of Naval Architecture and Ocean Engineering, University of Ulsan, 102 Daehakro, Ulsan 680-749, Republic of Korea

ARTICLE INFO

Article history:
Received 25 January 2009
Received in revised form
9 March 2009
Accepted 30 March 2009
Available online 12 April 2009

Keywords:
Surface tension
Free streamline flows
Brillouin–Villat criterion

ABSTRACT

Cavity flow past a circular cylinder is considered accounting for the surface tension on the cavity boundary. The fluid is assumed to be inviscid and incompressible, and the flow is assumed to be irrotational. The solution is based on two derived governing expressions, which are the complex velocity and the derivative of the complex potential defined in an auxiliary parameter region. An integral equation in the velocity magnitude along the free surface is derived from the dynamic boundary condition. The Brillouin–Villat criterion is employed to determine the location of the point of flow separation. The cases of zero surface tension and zero cavitation number are obtained as limiting cases of the solution. Numerical results concerning the effects of surface tension and cavitation development on the cavity detachment, the drag force and the geometry of the free boundaries are presented over a wide range of the Weber and the cavitation numbers.

1. Introduction

The study of cavity flows past curved bodies with surface tension started to receive much attention in 1970s owing to the development of hydrofoil sections for high-speed crafts, marine propellers and turbopumps designed to work under cavitation conditions. During that time, the application of the classical theory of free streamline flows failed to take into account any effects which surface tension might have on the free surface shape and the flow detachment point.

Important progress in the understanding of the influence of surface tension on the cavitating flow past a curved body was archived by Vanden-Broeck [1–3], who obtained a mathematical solution of the problem for zero cavitation number assuming that the contact angle between the free surface and the body may be different from zero. He found that the position of the separation point is uniquely determined by specifying the value of the Weber number and the contact angle at the separation point. In the last case, for a given value of the Weber number there is a particular position of the separation point for which the slope is continuous, the velocity magnitude is finite and the body and free surface curvatures are equal. This special case corresponds to the Brillouin–Villat criterion requiring a finite velocity throughout the flow region [4,5].

The experimental examination of free cavity detachment by Arakeri and Acosta [6] and Tassin Leger and Ceccio [7] for bluff body cavitation showed that the cavity detachment point was well downstream of that predicted by the classical model of ideal fluid. They found that the laminar boundary layer separation occurs upstream the cavity detachment and delays the cavity formation. The location of the boundary layer separation was a strong function of the cavitation number and a weak function of the Reynolds number.

Franc and Michel [8] examined flow over hydrofoils and also recognized the relationship between the boundary layer separation and the formation of attached cavitation. They proposed a new cavity detachment criterion based on the interaction of the inviscid cavity flow with the boundary layer upstream of the cavity detachment. They also drew attention to a paradox associated with the experimentally observed laminar flow separation. The paradox lies in the fact that the pressure gradient providing the laminar flow separation should be positive, whereas this is impossible assuming that the pressure in the cavity is the minimal pressure in the flow region.

From the above discussion it can be seen that there are two major factors influencing the cavity detachment, which are fluid viscosity and surface tension. At the moment, the contribution of each factor to the cavity detachment is still not fully understood. Obviously, the role of surface tension increases with decreasing body size or jet nozzle diameter. In industrial applications this occurs, for example, in ink jet printing [9], diesel injection systems [10] and hydroentangling nozzles in non-woven processing [11].

* Corresponding author.
E-mail addresses: bsyoon@ulsan.ac.kr (B.-S. Yoon), semenov@a-teleport.com (Y.A. Semenov).

0997-7546/$ – see front matter © 2009 Elsevier Masson SAS. All rights reserved.
doi:10.1016/j.euromechflu.2009.03.004

The role of surface tension in the cavity detachment has been investigated only for cases corresponding to open cavities and zero cavitation number. The problem under consideration becomes more complicated for the case of a non-zero cavitation number due to additional assumptions that are required to resolve the Brillouin paradox [12] and provide the closure of the cavity [13]. Besides, it is well known that an increase in the cavitation number affects the cavity length much more drastically than its width. This means that the curvature of the free surface and thus effects of surface tension may also increase at higher cavitation numbers.

In this paper we present an analytical solution of the problem of cavity flow past an arbitrarily shaped body in the presence of surface tension on the free boundaries for an arbitrary cavitation number. The analytical solutions corresponding to zero cavitation number and zero surface tension are obtained as special cases. The method of solution is based on deriving analytical expressions for the complex velocity and for the derivative of the complex potential, both defined in a parameter region. The expression for the complex velocity is obtained by using the integral formula [14] for solving the mixed boundary-value problem for the first quadrant. The derivative of the complex potential is obtained by using Chaplygin's singular point method [15,16]. The expression for the complex velocity contains two functions, which are the function of the slope of the tangent to the body and the function of the velocity magnitude along the free boundary. Such representation of the complex velocity makes it possible to directly apply the Brillouin–Villat condition to determine the location of minimal pressure, which may correspond to laminar flow separation or cavity detachment depending on whether or not the flow model takes account of the boundary layer. The solution is obtained in the form of a system of integro-differential equations in the aforementioned functions, which are derived from the dynamic and kinematic boundary conditions.

The formulation of the problem and the derivation of the governing expressions are discussed in Section 2. In Section 2.2 an implicit cavity closure model is presented. The model makes it possible to take into consideration both non-zero surface tension and non-zero cavitation numbers. The numerical procedure for solving the integro-differential equations and the numerical results corresponding to the flow past a circular cylinder are presented in Section 3. The dependences of the flow parameters on both the Weber and the cavitation number are discussed.

2. Statement of the problem

We consider the cavity flow of an inviscid incompressible fluid past a circular cylinder of radius R sketched in Fig. 1a taking into consideration the surface tension on the cavity boundary. We introduce Cartesian coordinates x and y and assume that the flow is symmetric about the x-axis. An implicit model of cavity closure is employed, for which the cavity contour OC is continued by the closing line CB. On the closing line the velocity magnitude is given as a function of the spatial coordinate s along the contour. As $s \to \infty$, this function tends to the velocity at infinity, U, and provides the closure of the cavity at infinity. This closure scheme in some sense simulates the viscous wake occurring downstream of the cavity in real flows [17].

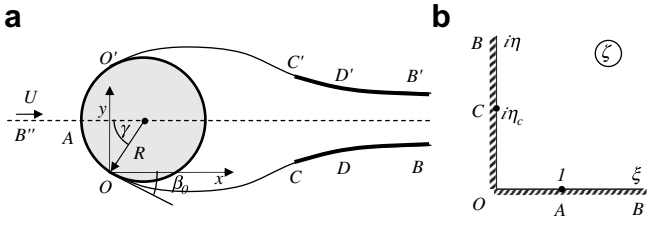

Fig. 1. Sketch of the cavity flow past a circular cylinder a) and parameter plane b).

Surface tension affects the pressure jump across the cavity boundary according to the Laplace–Young condition

$$p - p_c = \tau\chi, \tag{1}$$

where p_c is the pressure in the cavity, τ is the coefficient of surface tension, and χ is the curvature of the cavity boundary.

From the Bernoulli equation

$$\frac{V^2}{2} + \frac{p}{\rho} = \frac{U^2}{2} + \frac{p_\infty}{\rho}$$

and the Laplace–Young condition (1) we can express the magnitude of the velocity on the cavity boundary as follows

$$v = \frac{V}{U} = \sqrt{1 + \sigma - \frac{2\chi R}{We}}. \tag{2}$$

Here, σ is the cavitation number and We is the Weber number, which are defined as follows

$$\sigma = \frac{p_\infty - p_c}{1/2\rho U^2}, \quad We = \frac{\rho U^2 R}{\tau}, \tag{3}$$

where p_∞ is the pressure at infinity, and ρ is the liquid density.

Let us introduce the complex potential $w(z) = \phi(x,y) + i\psi(x,y)$ where $\phi(x,y)$ is the flow potential and $\psi(x,y)$ is the stream function, which is the harmonic conjugate of ϕ. If expressions for the complex conjugate velocity, dw/dz, and for the derivative of the complex potential, $dw/d\varsigma$, both defined in the parameter region ς, are known, then we obtain the solution of the problem in the parametric form [18]:

$$w(\varsigma) = w_0 + \int_0^\varsigma \frac{dw}{d\varsigma'}\,d\varsigma', \quad z(\varsigma) = z_0 + \int_0^\varsigma \frac{dw}{d\varsigma'}\Big/\frac{dw}{dz}\,d\varsigma' \tag{4}$$

where z_0 is the coordinate of point O, and w_0 is the chosen value of the complex potential at this point.

Let the first quadrant of the ς-plane, where the complex variable is $\varsigma = \xi + i\eta$, corresponds to the physical flow region. Conformal mapping allows us to fix three points O, A and B as shown in Fig. 1b, so that the interval $0 < \xi < 1$ of the real axis corresponds to the wetted part of the cylinder, and the interval $1 < \xi < \infty$ corresponds to the wall symmetry line CB''. The imaginary η-axis of the parameter region corresponds to the free boundary OCB including the cavity contour OC corresponding to $0 < \eta < \eta_c$ and the closure contour CB, for which $\eta_c < \eta < \infty$. Since the actual ranges of the complex velocity and complex potential are unknown *a priori*, an explicit conformal transformation of the first quadrant onto the complex velocity and complex potential planes is a difficult problem. At this stage, to find these functions, we assume that the magnitude of the velocity v and the slope β of the tangent to the wetted part of the body are known as functions of the parameter variables η and ξ, respectively.

2.1. Expressions for the complex velocity and for the derivative of the complex potential

Using the above definitions, the boundary conditions for the complex velocity, dw/dz, can be written as follows

$$\arg\left(\frac{dw}{dz}\right) = -\beta(\xi), \quad 0 < \xi < 1, \ \eta = 0,$$

$$\arg\left(\frac{dw}{dz}\right) = 0, \qquad 1 < \xi < \infty, \ \eta = 0,$$

$$\left|\frac{dw}{dz}\right| = v(\eta), \qquad 0 < \eta < \infty, \ \xi = 0. \tag{5}$$

The function $\beta(\xi)$ decreases when moving from point O to point A from the value $\beta(0) = \beta_0$ to the value $\beta(1) = -\pi/2$. The problem is then to find the function dw/dz in the first quadrant of the parameter plane which satisfies the boundary conditions (5). The formula [14]

$$\frac{dw}{dz} = v_0 \exp\left[\frac{1}{\pi}\int_0^\infty \frac{d\beta}{d\xi'}\ln\left(\frac{\varsigma-\xi'}{\varsigma+\xi'}\right)d\xi' - \frac{i}{\pi}\int_0^\infty \frac{d\ln v}{d\eta'}\ln\left(\frac{i\eta'-\varsigma}{i\eta'+\varsigma}\right)d\eta'\right], \tag{6}$$

provides the solution of the mixed boundary-value problem (5). It can be easily verified that for $\varsigma = \xi$ the argument of the function dw/dz is the function $\beta(\xi)$ while for $\varsigma = i\eta$ the magnitude of dw/dz is the function $v(\eta)$, i.e. the boundary conditions (5) are satisfied.

The argument of the complex velocity undergoes a step change at point A ($\varsigma = 1$), which corresponds to the angle between the cylinder surface and the axis of symmetry. Evaluating the first integral over the step change at the point $\varsigma = 1$, $\beta(1+\varepsilon) - \beta(1-\varepsilon) = \pi/2$, where $\varepsilon \to 0$, we finally obtain the expression for the complex velocity

$$\frac{dw}{dz} = v_0\left(\frac{\varsigma-1}{\varsigma+1}\right)^{1/2} \exp\left[\frac{1}{\pi}\int_0^1 \frac{d\beta}{d\xi'}\ln\left(\frac{\varsigma-\xi'}{\varsigma+\xi'}\right)d\xi' - \frac{i}{\pi}\int_0^\infty \frac{d\ln v}{d\eta'}\ln\left(\frac{i\eta'-\varsigma}{i\eta'+\varsigma}\right)d\eta'\right]. \tag{7}$$

An explicit expression for the derivative of the complex potential can be obtained by using the conformal mapping method because the region of the complex potential w is just a half-plane of the w-plane, i.e. $-\infty < \varphi < \infty$, $\psi = 0$. There is only one point, $\varsigma = 0$, where the mapping of the first quadrant onto the w-plane is not conformal. Thus the complex potential $w(\varsigma)$ has a singularity at the point $\varsigma = 0$, where its local behavior is $w \sim K\varsigma^2$, K being a real constant. There are no other points in the ς-plane where the mapping is not conformal. Thus, the derivative of the complex potential takes the form

$$\frac{dw}{d\varsigma} = K\varsigma. \tag{8}$$

Dividing (8) by (7), we derive the expression

$$\frac{dz}{d\varsigma} = \frac{K\varsigma}{v_0}\left(\frac{\varsigma+1}{\varsigma-1}\right)^{1/2} \exp\left[-\frac{1}{\pi}\int_0^1 \frac{d\beta}{d\xi'}\ln\left(\frac{\varsigma-\xi'}{\varsigma+\xi'}\right)d\xi' + \frac{i}{\pi}\int_0^\infty \frac{d\ln v}{d\eta'}\ln\left(\frac{i\eta'-\varsigma}{i\eta'+\varsigma}\right)d\eta'\right], \tag{9}$$

whose integration in equation (4) gives the function $z(\varsigma)$ which conformally maps the first quadrant of the parameter plane onto the flow region in the z-plane. The integration along the imaginary axis of the parameter region provides the free surface of the flow. The parameter K and the functions $\beta(\xi)$ and $v(\eta)$ are determined from the boundary conditions and from physical considerations.

The spatial coordinate s along the free surface, $s = s(\eta)$, and along the wetted part of the cylinder, $s = s(\xi)$, is determined as follows

$$s(\eta) = -\int_0^\eta \left|\frac{dz}{d\varsigma}\right|_{\varsigma = i\eta} d\eta = -K\int_0^\eta \frac{\eta}{v(\eta)}\,d\eta, \tag{10}$$

$$s(\xi) = \int_0^\xi \left|\frac{dz}{d\varsigma}\right|_{\varsigma = \xi} d\xi. \tag{11}$$

The real factor K is determined from the condition for the length of the wetted part of the cylinder $S_w = R\gamma$. By substituting equation (9) into (11), we obtain

$$S_w = \frac{K}{v_0}\int_0^1 \xi\left(\frac{\xi+1}{1-\xi}\right)^{\frac{1}{2}} \exp\left[-\frac{1}{\pi}\int_0^1 \frac{d\beta}{d\xi'}\ln\left|\frac{\xi-\xi'}{\xi+\xi'}\right|d\xi' - \frac{1}{\pi}\int_0^\infty \frac{d\ln v}{d\eta'}\left(\pi - 2\tan^{-1}\frac{\eta'}{\xi}\right)d\eta'\right]d\xi. \tag{12}$$

2.2. Cavity closure model

Within the framework of the model of ideal fluid the formulation of the cavity flow problem with non-zero cavitation numbers is not unique due to the Brillouin paradox [12]. As a way to resolve this paradox, additional assumptions as to the flow in the cavity closure region are necessary. The assumptions made by Roshko, Riabouchinsky, Efros in his re-entrant jet model, Tulin, etc. are now well known as classical models of cavity flows [16]. These models provide close results for developed cavitating flows, for which the cavity re-closes downstream of the cavitating object. In cases where the size of the cavity is comparable with the body size or the cavity surface re-closes on the solid surface of the cavitating object (partial cavitation) different assumptions made in the cavity closure region lead to different results. Besides, there are some differences in the formulation of the problems of partial and developed cavitation, which makes it difficult to study the transition from developed to partial cavitation.

The model of viscous cavity flow [17] based on the viscous/inviscid interaction approach proposed by Crocco and Lees [19] takes into consideration viscous effects of the fluid, which manifest themselves significantly in the cavity closure region. In that model, the velocity magnitude on the boundary of the outer inviscid flow consisting of the cavity surface and the displacement thickness of the viscous wake is determined from the Bernouli equation and equations modeling the flow in the wake region, respectively. In the present work aimed to study the surface tension effects, we drop the model of the viscous wake and introduce an assumption as to the velocity distribution along the wake.

It is assumed for simplicity that the velocity magnitude, $v(s)$, on the cavity closure contour CDB linearly decreases from the value v_c determined by equation (2) at the point of separation C to the value U at infinity (point D)

$$v(s') = \begin{cases} v_c\dfrac{s'_C + S_{CD} - s'}{S_{CD}} + U\dfrac{s' - s'_C}{S_{CD}}, & s'_C \le s' \le s'_C + S_{CD} \\ U, & s'_C + S_{CD} < s' < \infty \end{cases} \tag{13}$$

where $s' = -s > 0$, and S_{CD} is the given length between points C and D.

The cavity closure condition requires that the y-coordinates of the free surface at infinity on the right and left sides be the same, that is

$$\mathrm{Im}\left(\oint_{\varsigma=\infty}\frac{\mathrm{d}z}{\mathrm{d}\varsigma}\mathrm{d}\varsigma\right)=-\mathrm{Im}\left(\oint_{\varsigma'=0}\frac{\mathrm{d}z}{\mathrm{d}\varsigma'}\frac{\mathrm{d}\varsigma'}{\varsigma'^2}\right)=-\frac{\mathrm{i}\pi}{4}\underset{\varsigma'=0}{res}\frac{\mathrm{d}^2}{\mathrm{d}\varsigma'^2}\left(\frac{\mathrm{d}z}{\mathrm{d}\varsigma'}\varsigma'\right)=0, \tag{14}$$

where $\varsigma'=1/\varsigma$.

By evaluating the integral using the theorem of residues, we get the following equation

$$\int_0^1\frac{\mathrm{d}\beta}{\mathrm{d}\xi'}\,\xi'\,\mathrm{d}\xi'+\int_0^\infty\frac{\mathrm{d}\ln v}{\mathrm{d}\eta'}\,\eta'\,\mathrm{d}\eta'+\frac{\pi}{2}=0. \tag{15}$$

The magnitude of the velocity $v(\eta)=v[s(\eta)]$, $\eta_C<\eta<\infty$, on the closure contour CD given by equation (13) affects the second integral in equation (15). By finding an appropriate value of the coordinate $s_C=s(\eta_C)$, which determines the cavity length, equation (15) can be satisfied.

2.3. Condition for flow separation

The problem of cavity flow with surface tension past a circular cylinder was investigated widely by Vanden-Broeck [1–3] for the case of zero cavitation number. He found that there exists only one angular position γ^* of the flow separation point for which the velocity takes a finite value at this point. For $\gamma<\gamma^*$ the velocity at the separation point tends to infinity, and therefore its derivative $\mathrm{d}v/\mathrm{d}s<0$. Here, s is the spatial coordinate along the cylinder surface measured from the separation point. For the case $\gamma>\gamma^*$ the velocity at the separation point tends to zero, and therefore $\mathrm{d}v/\mathrm{d}s>0$. Since the velocity takes a finite value for $\gamma=\gamma^*$, $\mathrm{d}v/\mathrm{d}s$ should be equal to zero at the separation point. This is the formulation of the Brillouin–Villat condition [16,12] determining the location of flow separation. From the above discussion we can conclude that this condition also retains its form for the problem under consideration, i.e.

$$\lim_{s\to0}\frac{\mathrm{d}\ln v}{\mathrm{d}s}=0, \tag{16}$$

where s is the spatial coordinate along the body.

By using the relation $\mathrm{d}(\ln v)/\mathrm{d}s=(\mathrm{d}(\ln v)/\mathrm{d}\xi)/(\mathrm{d}s/\mathrm{d}\xi)$ and differentiating the function $v(\xi)=|\mathrm{d}w/\mathrm{d}z|_{\varsigma=\xi}$ determined by equation (6), the condition (16) takes the form

$$\int_0^1\frac{\mathrm{d}\beta}{\mathrm{d}\xi'}\frac{\mathrm{d}\xi'}{\xi'}-\int_0^\infty\frac{\mathrm{d}\ln v}{\mathrm{d}\eta'}\frac{\mathrm{d}\eta'}{\eta'}+\frac{\pi}{2}=0. \tag{17}$$

This is an equation in the unknown length of the wetted part of the foil, S_w, which affects the function $\beta(\xi)=\beta[s(\xi)]$, $0<s<S_w$.

2.4. Integro-differential equations in the functions $\beta(\xi)$ and $v(\eta)$

Since the function $\beta(s)$ is given by the body shape, the function $\beta(\xi)$, in view of equation (10), is determined from the following integro-differential equation

$$\frac{\mathrm{d}\beta}{\mathrm{d}\xi}=\frac{\mathrm{d}\beta}{\mathrm{d}s}\frac{\mathrm{d}s}{\mathrm{d}\xi}=\chi[s(\xi)]\,\frac{K\xi}{v_0}\left(\frac{1+\xi}{1-\xi}\right)^{\frac12}\exp\left[-\frac{1}{\pi}\int_0^1\frac{\mathrm{d}\beta}{\mathrm{d}\xi'}\ln\left(\frac{\xi'-\xi}{\xi'+\xi}\right)\mathrm{d}\xi'\right.$$
$$\left.-\frac{1}{\pi}\int\frac{\mathrm{d}\ln v}{\mathrm{d}\eta'}\ln\left(\pi-2\tan^{-1}\left(\frac{\eta'}{\xi}\right)\right)\mathrm{d}\eta'\right], \tag{18}$$

where $\chi(s)$ is the curvature of the body given as a function of the arc length s.

In order to derive an integral equation in the function $v(\eta)$, we first need to get an expression for the curvature χ along the cavity boundary, i.e. along the imaginary axis η of the parameter region. The slope of the free surface is determined from equation (7) as follows

$$\gamma(\eta)=-\arg\left(\frac{\mathrm{d}w}{\mathrm{d}z}\right)=\tan^{-1}\eta-\pi/2-\frac{1}{\pi}\int_0^1\frac{\mathrm{d}\beta}{\mathrm{d}\xi'}\left(\pi-2\tan^{-1}\left(\frac{\eta}{\xi'}\right)\right)\mathrm{d}\xi'$$
$$+\frac{1}{\pi}\int_0^\infty\frac{\mathrm{d}\ln v}{\mathrm{d}\eta'}\ln\left|\frac{\eta'-\eta}{\eta'+\eta}\right|\mathrm{d}\eta'$$

Differentiating the above equation and taking into account equation (10), we find the curvature of the free surface

$$\chi=\frac{\mathrm{d}\gamma/\mathrm{d}\eta}{\mathrm{d}s/\mathrm{d}\eta}=-\frac{v}{K\eta}\left(\frac{1}{1+\eta^2}+\frac{2}{\pi}\int_0^1\frac{\mathrm{d}\beta}{\mathrm{d}\xi'}\frac{\xi'\,\mathrm{d}\xi'}{\xi'^2+\eta^2}-\frac{2}{\pi}\int_0^\infty\frac{\mathrm{d}\ln v}{\mathrm{d}\eta'}\frac{\eta'\,\mathrm{d}\eta'}{\eta'^2-\eta^2}\right). \tag{19}$$

By substituting equation (19) into the dynamic boundary condition (2), we obtain the following integral equation in the function $\mathrm{d}\ln v/\mathrm{d}\eta$

$$\frac{2}{\pi}\int_0^\infty\frac{\mathrm{d}\ln v}{\mathrm{d}\eta'}\frac{\eta'\,\mathrm{d}\eta'}{\eta'^2-\eta^2}=\frac{1}{1+\eta^2}+\frac{2}{\pi}\int_0^1\frac{\mathrm{d}\beta}{\mathrm{d}\xi'}\frac{\xi'\,\mathrm{d}\xi'}{\xi'^2+\eta^2}+\frac{WeK\eta}{2Rv}\left(1+\sigma-v^2\right), \tag{20}$$

where

$$v(\eta)=v_0\exp\left(\int_0^\eta\frac{\mathrm{d}\ln v}{\mathrm{d}\eta'}\mathrm{d}\eta'\right)\quad\text{and}\quad v_0=\sqrt{1+\sigma+2/We}$$

2.5. Curvature of the free surface at the point of separation

In order to evaluate the curvature of the free surface at the separation point, where at $\eta=0$ equation (19) has an indeterminate form, we differentiate the numerator and denominator of equation (19) to obtain:

$$\chi_0=\lim_{\eta\to0}\left\{-\frac{1}{K}\frac{\mathrm{d}v}{\mathrm{d}\eta}\left(\frac{1}{1+\eta^2}+\frac{2}{\pi}\int_0^\infty\frac{\mathrm{d}\beta}{\mathrm{d}\xi'}\frac{\xi'\,\mathrm{d}\xi'}{\xi'^2+\eta^2}\right.\right.$$
$$\left.\left.-\frac{2}{\pi}\int_0^\infty\frac{\mathrm{d}\ln v}{\mathrm{d}\eta'}\frac{\eta'\,\mathrm{d}\eta'}{\eta'^2-\eta^2}\right)\right\}+\lim_{\eta\to0}\left\{\frac{2\eta v}{K}\left(\frac{1}{(1+\eta^2)^2}\right.\right.$$
$$\left.\left.+\frac{2}{\pi}\int_0^\infty\frac{\mathrm{d}\beta}{\mathrm{d}\xi'}\frac{\xi'\,\mathrm{d}\xi'}{(\xi'^2+\eta^2)^2}+\frac{2}{\pi}\int_0^\infty\frac{\mathrm{d}\ln v}{\mathrm{d}\eta'}\frac{\eta'\,\mathrm{d}\eta'}{(\eta'^2-\eta^2)^2}\right)\right\} \tag{21}$$

The first term in the above equation equals zero due to the flow separation condition (17). In order to evaluate the second term containing the singular integrals, we have to estimate the behavior of the functions $\mathrm{d}\ln v/\mathrm{d}\eta$ at $\eta\to0$ and $\mathrm{d}\beta/\mathrm{d}\xi$ at $\xi\to0$. From the Brillouin–Villat condition (16) it follows

$$\frac{\mathrm{d}\ln v}{\mathrm{d}s}=\frac{\mathrm{d}\ln v}{\mathrm{d}\eta}\Big/\frac{\mathrm{d}s}{\mathrm{d}\eta}=0.$$

In view of equation (10), it can be seen that for $\eta\to 0$ $\mathrm{d}s/\mathrm{d}\eta = K\eta/v(\eta)\sim\eta$. Therefore, from equation (16) it follows

$$\lim_{\eta\to 0}\frac{\mathrm{d}\ln v}{\mathrm{d}\eta}\frac{1}{\eta}=0,\quad\Rightarrow\quad\frac{\mathrm{d}\ln v}{\mathrm{d}\eta}\sim\eta^{1+\alpha},\quad\eta\to 0,\quad\alpha\geq 0. \tag{22}$$

The behavior of the function $\mathrm{d}\beta/\mathrm{d}\xi$ is determined in a similar way

$$\frac{\mathrm{d}\beta}{\mathrm{d}\xi}=\frac{\mathrm{d}\beta}{\mathrm{d}s}\frac{\mathrm{d}s}{\mathrm{d}\xi}=-\frac{1}{R}\frac{\mathrm{d}s}{\mathrm{d}\xi}=-\frac{1}{R}\frac{K\xi}{v(\xi)},\quad\Rightarrow\quad\frac{\mathrm{d}\beta}{\mathrm{d}\xi}\sim-\frac{K}{Rv_0}\xi, \tag{23}$$

where $v_0=\lim_{\xi\to 0}v(\xi)=\lim_{\xi\to 0}|\mathrm{d}w/\mathrm{d}z|_{\varsigma=\xi}$, and R is the radius of the cylinder.

By substituting the estimates (22) and (23) of the functions $\mathrm{d}\ln v/\mathrm{d}\eta$ and $\mathrm{d}\beta/\mathrm{d}\xi$ into the corresponding integrals in equation (21) and taking into account that

$$\lim_{\eta\to 0}\eta\int_0^\infty\frac{\eta'^2\,\mathrm{d}\eta'}{\left(\eta'^2-\eta^2\right)^2}=0\quad\text{and}\quad\lim_{\eta\to 0}\eta\int_0^\infty\frac{\xi'^2\,\mathrm{d}\xi'}{\left(\xi'^2+\eta^2\right)^2}=\frac{\pi}{4},$$

we can find that the curvature of the free surface at the point of flow separation is equal to the curvature of the body, i.e.

$$\chi_0=\lim_{\eta\to 0}\chi(\eta)=-\frac{1}{R}. \tag{24}$$

3. Numerical method and results

The body shape is chosen to be a circular cylinder of radius R, the length of the closure interval being related to R as $S_{CD}/R=10$. In discrete form, the solution is sought on a fixed set of points ξ_j, $j=1,\ldots,M$ distributed along the real axis of the parameter region and on a fixed set of points η_j, $j=1,\ldots,N$ distributed along its imaginary axis. The total number of points η_j was chosen in the range $N=25$–200, and the total number of points ξ_j was chosen in the range $M=3N$ to check the convergence of the solution procedure. The points ξ_j are distributed so as to provide a higher density of the points $s_j=s(\xi_j)$ at points O and A, at which the derivative $\mathrm{d}s/\mathrm{d}\xi=|\mathrm{d}z/\mathrm{d}\varsigma|_{\varsigma=\xi}$ has singularities. The distribution of the points η_j is chosen so as to provide a higher density of the points $s_j=s(\eta_j)$ on the free surface near the point of flow separation.

The solution of equations (20) was found by the method of successive approximations applying the Hilbert transform to determine the $(k+1)$th approximation

$$\left(\frac{\mathrm{d}\ln v}{\mathrm{d}\eta}\right)^{(k+1)}=\frac{4}{\pi^2}\int_0^\infty F^{(k)}(\eta')\frac{\eta'\,\mathrm{d}\eta'}{\left(\eta'^2-\eta^2\right)}, \tag{25}$$

where

$$F^{(k)}(\eta)=\frac{1}{1+\eta^2}+\frac{2}{\pi}\int_0^1\left(\frac{\mathrm{d}\beta}{\mathrm{d}\xi'}\right)^{(k)}\frac{\xi'\mathrm{d}\xi'}{\xi'^2+\eta^2}+\frac{WeK\eta}{2Rv^{(k)}}\left(1+\sigma-\left(v^{(k)}\right)^2\right), \tag{26}$$

$$v^{(k)}(\eta)=v_0\exp\left(\int_0^\eta\left(\frac{\mathrm{d}(\ln v)}{\mathrm{d}\eta'}\right)^{(k)}\mathrm{d}\eta'\right).$$

In each iteration step k the integro-differential equation (18) in the function $\mathrm{d}\beta/\mathrm{d}\xi$ was solved using the inner iteration procedure

$$\left(\frac{\mathrm{d}\beta}{\mathrm{d}\xi}\right)^{(l+1)}=\chi\left[s^{(l)}(\xi)\right]\frac{K^{(l)}\xi}{v_0}\left(\frac{1+\xi}{1-\xi}\right)^{\frac{1}{2}}\exp\left[-\frac{1}{\pi}\int_0^1\left(\frac{\mathrm{d}\beta}{\mathrm{d}\xi'}\right)^{(l)}\ln\left(\frac{\xi'-\xi}{\xi'+\xi}\right)\mathrm{d}\xi'-\frac{1}{\pi}\int_0^\infty\left(\frac{\mathrm{d}\ln v}{\mathrm{d}\eta'}\right)^{(k)}\left(\pi-2\tan^{-1}\left(\frac{\eta'}{\xi}\right)\right)\mathrm{d}\eta'\right], \tag{27}$$

where the curvature $\chi(s)\equiv -1/R$ for the case of the circular cylinder.

In each iteration step l the parameters $K^{(l)}$, η_C and $S_w=\gamma R$ were calculated from equation (12), (15) and (17), respectively. The integrals appearing in the system of equations were evaluated using the linear interpolation of the functions $\beta(\xi)$ and $\mathrm{d}(\ln v)/\mathrm{d}\eta$ on the intervals (ξ_{j-1},ξ_j) and (η_{j-1},η_j), respectively. In the first iteration the functions $\beta(\xi)$ and $(\mathrm{d}\ln v)/\mathrm{d}\eta$ were given as $\beta(\xi)\equiv 0$ and $v(\eta)\equiv 1$.

The convergence of the inner iteration procedure required 5–10 iterations to reach the condition $|(\mathrm{d}\beta/\mathrm{d}\xi)_j^{l+1}-(\mathrm{d}\beta/\mathrm{d}\xi)_j^l|<\varepsilon$, $j=1,\ldots,M$, for the chosen value $\varepsilon=10^{-7}$. The convergence of the outer iterations required from several hundreds to several thousands of iterations, and it was obtained applying the under-relaxation method.

3.1. Validation of the numerical procedure

With the aim to estimate the accuracy of the results for finite Weber numbers, in Table 1 the calculated angles of flow separation are presented for four numbers of nodes on the free surface. The difference between the results corresponding to different numbers of nodes decreases with the number of nodes, thus showing the convergence of the numerical results to the solution of the problem. The accuracy slightly decreases as the Weber number decreases. However, the difference between the results corresponding to $N=100$ and 200 is about 0.1%, which is rather good for this kind of problems.

For validation purposes, Table 2 compares the angles of flow separation and the drag coefficients for zero surface tension and number of nodes $N=100$ with the results presented in Gurevich [16]. Some difference, which is less than 1.2%, occurs for larger cavitation numbers.

3.2. Effect of the Weber and the cavitation numbers on the flow parameters

In Table 3, the solutions are presented in terms of the angle of cavity detachment γ, the drag coefficient C_x, and the cavity length l_c. For the case of zero cavitation number the cavity length is not shown since it takes an infinite value. From the results it can be seen that as the Weber number decreases, the angle γ increases while the drag coefficient and the cavity length decrease.

Table 1
Effect of the number of nodes on the angle of separation for different Weber numbers at zero cavitation number.

We	$N=25$	$N=50$	$N=100$	$N=200$
10^5	54.56	54.94	55.02	55.04
10^2	55.05	55.83	56.03	56.05
10	58.70	61.04	61.76	61.81
5	61.7	65.08	65.98	66.05
3	64.85	69.11	70.23	70.30
2	67.83	72.93	74.24	74.31

Table 2
The flow separation angles and drag coefficients for various cavitation numbers compared with the data presented in Gurevich [16].

σ	Present	γ, deg. [16]	Present	C_x [16]
0	55.02	55.04	0.4986	0.4986
0.1	55.11	55.13	0.5493	0.5493
0.2	55.39	55.37	0.6018	0.6016
0.3	55.78	55.73	0.6560	0.6553
0.5	56.84	56.70	0.7696	0.7677
0.8	59.00	58.61	0.9536	0.9476
1.0	60.84	60.11	1.0847	1.0751

The cavitation number affects the angle of cavity detachment and the drag coefficient only slightly while the cavity length depends more significantly on both these parameters. It should be noted that the cavity length depends slightly on the cavity closure model too, namely, on the length of the interval S_{CD} and the velocity distribution along this interval. It can be seen from equation (15) that the second integral depends on the velocity distribution $v(\eta)$ along the line CDB' corresponding to the interval $\eta_C < \eta < \infty$ on the imaginary axis of the parameter plane. The results presented in Table 3 were obtained for the velocity distribution along the closure line given by equation (13).

Fig. 2 shows the cavity contours for cavitation numbers $\sigma = 0$ (a) and $\sigma = 0.2$ (b) and different Weber numbers. It can be seen that the wetted part of the cylinder becomes larger and the cavity width becomes smaller as the Weber number decreases. For cavitation number $\sigma = 0$ and Weber number $We = 0.8$ the cavity boundary reaches the symmetry line at $x \approx 4$. From a mathematical viewpoint, the solution can exist for $We < 0.8$, but for physical reasons this is the limit Weber number corresponding to zero cavitation number and an infinite cavity length. For Weber number $We = 0.6$, the cavity boundary reaches the symmetry line closer to the cylinder at $x \approx 2$. Such behavior confirms Vanden-Broeck's results [2], according to which the cavity length tends to zero as $We \to 0$.

Another feature is that the curvature may reverse when moving along the cavity boundary. However, the magnitude of the curvature decreases and tends to zero at infinity. Ackerberg's solution [20] contains waves on the free surface downstream. Cumberbatch and Norbury [21] have noted that these waves are not physically acceptable because they require a supply of energy from infinity.

The solution presented here shows that the amplitude of the waves rapidly decreases. This can be seen more clearly from the behavior of the curvature along the cavity boundary shown in Fig. 3. For near-zero surface tension ($We = 10^5$), the curvature monotonically increases from the value of the cylinder curvature at the detachment point to zero at infinity. For Weber numbers $We > 10$,

Table 3
Effect of the Weber and the cavitation numbers on the angle of cavity detachment, the drag coefficient, and the cavity length.

We	$\sigma = 0$		$\sigma = 0.2$			$\sigma = 0.5$		
	γ	C_x	γ	C_x	S_C	γ	C_x	S_C
10^5	55.02	0.4986	55.39	0.6017	42.0	56.84	0.7695	4.49
10^3	55.12	0.4983	55.47	0.6015	42.0	56.91	0.7692	4.49
10^2	56.03	0.4957	56.36	0.5989	41.4	57.63	0.7668	4.38
30	57.82	0.4878	57.79	0.5913	40.1	58.88	0.7596	4.13
10	61.76	0.4596	61.25	0.5643	36.6	61.93	0.7346	3.42
7	63.68	0.4385	63.05	0.5443	34.2	63.58	0.7161	2.97
5	65.98	0.4084	65.12	0.5155	31.3	65.51	0.6896	2.39
4	67.74	0.3804	66.72	0.4888	28.6	67.03	0.6651	1.91
3	70.23	0.3322	69.07	0.4425	24.9	69.34	0.6226	1.15
2.5	71.97	0.2928	70.72	0.4043	21.8	–	–	–
2	74.24	0.2329	72.99	0.3457	17.5	–	–	–

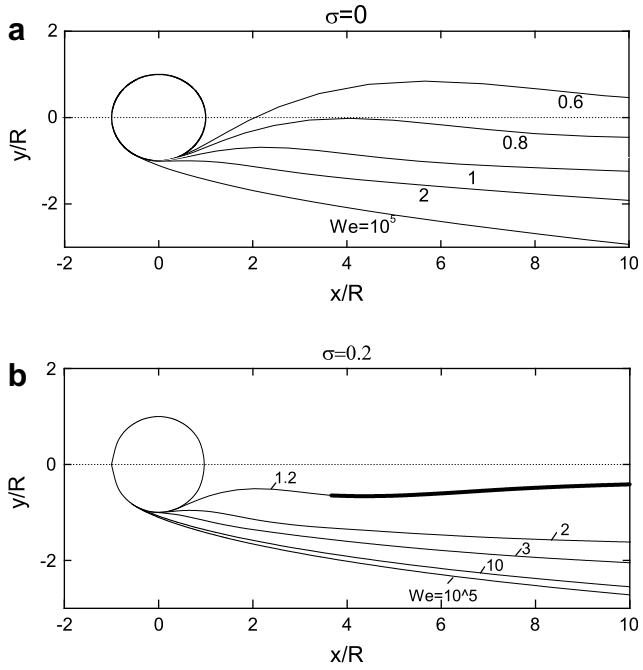

Fig. 2. Effect of surface tension on the cavity shape for cavitation number $\sigma = 0$ (a) and for $\sigma = 0.2$ (b). The cavity contours are shown by thin lines; the cavity closure contour for $We = 1.2$ in (b) is shown by a thick line. For larger Weber numbers the cavity lengths exceed the plot area of figure (b).

the curvature behaves like a wave close to the separation point. However, it remains negative along the cavity, so the wave on the free surface does not appear. For larger surface tension ($We < 10$), an interval in which the cavity curvature becomes positive appears on the cavity boundary. The length of this interval increases with increasing surface tension (decreasing Weber number). This reversal of sense of the curvature for Weber numbers less than 10 can also be seen from the shape of the cavity boundaries in Fig. 2.

Fig. 4 shows the cavity length l_c and the drag coefficient C_x versus the Weber number at cavitation number $\sigma = 0.2$. It can be seen that for $We > 20$ the effect of surface tension on the flow parameters is quite small. For lower Weber numbers the drag coefficient decreases with decreasing Weber number.

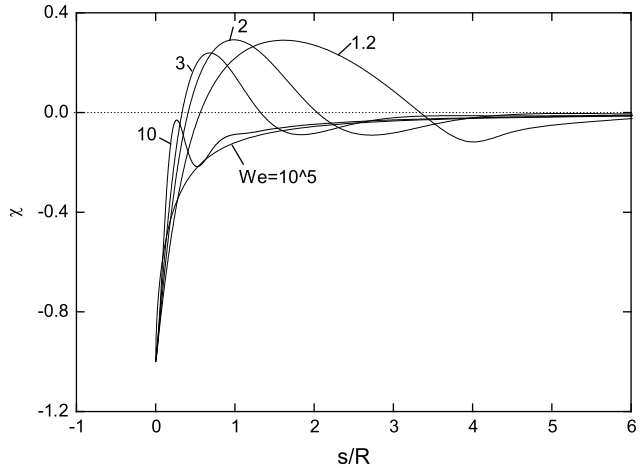

Fig. 3. Effect of surface tension on the curvature of the free surface at zero cavitation number.

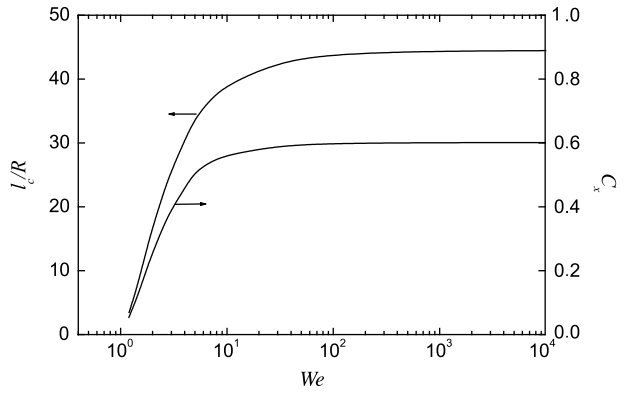

Fig. 4. Effect of surface tension on the cavity length and the drag coefficient at cavitation number $\sigma = 0.2$.

In the present formulation of the problem there is a pressure jump along the cylinder surface at the separation point. Indeed, the pressure in the cavity is p_c and the pressure on the cylinder surface near the separation point is $p = p_c + \tau\chi_0 < p_c$. By introducing the pressure coefficient

$$C_p = \frac{p - p_c}{1/2\rho U^2}$$

we can determine from equation (1) the jump in the pressure coefficient at the separation point $C_p = -2/We$. The smaller the Weber number, the larger the wetted part of the cylinder where the pressure is negative, which causes the drag coefficient to decrease. In real flows the pressure jump does not occur. However, there is a small region of a positive pressure gradient downstream corresponding to the separated laminar boundary layer, which occupies some room upstream of the cavity detachment [6].

The solution presented above may be used as a solution for the outer inviscid flow within the framework of the viscous/inviscid interaction approach. From the solution it is possible to determine the displacement thickness of the viscous layer, which is the distance between the boundary of the inviscid flow (cavity boundary in the present formulation) and the body. The boundary layer theory [22] makes it possible to determine the velocity magnitude at the outer boundary of the viscous layer if the displacement thickness is given. The determined magnitude of the velocity is used in the boundary conditions (5) instead of that obtained from the Bernoulli equation (condition (2)). By repeating the solution process for the outer flow, we can determine a refined location of the inviscid boundary and thus a refined displacement thickness. In this approach, the point of minimal pressure determined from the Brillouin–Villat condition will correspond to the separation point of the laminar boundary layer [7].

4. Conclusions

The problem of cavity flow past a circular cylinder with due regard for the surface tension and cavitation effects has been solved using an advanced hodograph method of complex analysis. Analytical expressions for the flow potential and for the function that conformally maps the parameter region onto the flow region have been obtained in integral form containing the velocity magnitude along the free surface and the slope of the tangent to the wetted part of the body, both as functions of the parameter variable. A system of integro-differential equations in these two functions has been derived from the dynamic and kinematic boundary conditions.

An equation determining the cavity detachment point is found in explicit form by applying the Brillouin–Villat condition to the expression for the complex velocity.

The flow parameters have been investigated over a wide range of the Weber and the cavitation numbers. The numerical results show that for Weber numbers larger than 20 the effect of surface tension on the flow parameters is too small. For lower Weber numbers, the surface tension reduces the cavity length and the drag coefficient while the length of the wetted part of the cylinder increases.

At the separation point, the curvature of the free surface is equal to the curvature of the body, and its magnitude takes its maximal value. From this point on, the curvature increases up to some maximal value, which may be positive. At some low values of the Weber number, an intersection of the upper and lower free surfaces may occur, which limits the range of applicability of the present formulation of the problem.

Acknowledgements

The authors are thankful to Jean-Marc Vanden-Broeck, who read this manuscript and suggested several important improvements. The financial support of the present study provided by the University of Ulsan is gratefully acknowledged.

References

[1] J.-M. Vanden-Broeck, The influence of surface tension on cavitating flow past a curved obstacle, J. Fluid Mech. 133 (1983) 255–264.
[2] J.-M. Vanden-Broeck, Cavitating flow of a fluid with surface tension past a circular cylinder, Phys. Fluids A 3 (1991) 263–266.
[3] J.-M. Vanden-Broeck, Nonlinear capillary free-surface flows, J. Eng. Math. 50 (2004) 415–426.
[4] M. Brillouin, Les surfaces de glissement de Helmholtz et la resistance des fluids Ann, Chim. Phys. 23 (1911) 145–230.
[5] H. Villat, Sur la validite des solutions de certains problemes d'hydrodynamique, J. Math Pure Appl. 20 (1914) 231–290.
[6] V.H. Arakeri, A.J. Acosta, Viscous effects in the inception of cavitation on axisymmetric bodies, Trans. ASME J. Fluids Eng. 95 (1973) 519–527.
[7] A. Tassin Leger, S.L. Ceccio, Examination of the flow near the leading edge of attached cavitation. Part 1. Detachment of two-dimensional and axisymmetric cavities, J. Fluid Mech. 376 (1998) 61–90.
[8] J.P. Franc, J.M. Michel, Attached cavitation and the boundary layer: experimental investigation and numerical treatment, J. Fluid Mech. 154 (1985) 63–90.
[9] S.C. Titcomb, Dynamic surface tension of jet inks, Indust. Eng. Chem. Prod. Res. Develop. 20 (4) (1981) 680–684.
[10] C. Dongiovanni, R. Roberto, C. Negri, A fluid model for simulation of diesel injection systems in cavitating and non-cavitating conditions, ASME Int. Combust. Eng. Div. 40 (2003) 87–95.
[11] N. Anantharamaiah, H.V. Tafreshi, B. Pourdeyhimi, Numerical simulation of the formation of constricted waterjets in hydroentangling nozzles: effects of nozzle geometry, Chem. Eng. Res. Des. 84 (3A) (2006) 231–238.
[12] G. Birkhof, E.H. Zarantonello, Jets, Wakes and Cavities, Academic Press, New York, 1957.
[13] A.G. Terentiev, V.P. Zhitnikov, Stationary two-dimensional inviscid flow with flexible boundaries including the effect of surface tension, J. Eng. Math. 55 (2006) 111–126.
[14] O.M. Faltinsen, Y.A. Semenov, Nonlinear problem of flat-plate entry into an incompressible liquid, J. Fluid Mech. 611 (2008) 151–173.
[15] S.A. Chaplygin, About Pressure of a Flat Flow on Obstacles. On the Airplane Theory, Moscow Univ., 1910.
[16] M.I. Gurevich, Theory of Jets in Ideal Fluids, Academic Press, New York, 1965.
[17] Y.A. Semenov, Y. Tsujimoto, A cavity wake model based on the viscous/inviscid interaction approach and its application to non-symmetric cavity flows in inducers, Trans. ASME J. Fluids Eng. 125 (5) (2003) 758–766.
[18] N.E. Joukovskii, Modification of Kirchoff's method for determination of a fluid motion in two directions at a fixed velocity given on the unknown streamline, Math. Coll. 15 (1890) 121–278.
[19] L. Crocco, L. Lees, A mixing theory for the interaction between dissipative flows and nearly isentropic streams, J. Aerosol Sci. 19 (10) (1952) 649–676.
[20] R.C. Ackerberg, The effects of capillarity on free-streamline separation, J. Fluid Mech. 70 (part 2) (1975) 333–352.
[21] E. Cumberbatch, J. Norbury, Capillary modification of the singularity at a free-streamline separation point, Q. J. Mech. Appl. Math. 32 (1979) 303–312.
[22] H. Schlichting, Boundary Layer Theory, McGraw-Hill, New York, 1960.